JPE 9-6-5

Variable Structure PWM Controller for Highly Efficient PV Inverters

Seong-Jin Oh† and Myoung-Ho Sunwoo*

†*Dept. of Automotive Engineering, Hanyang University, Seoul, Korea

ABSTRACT

In general, the output voltage level of a PV array varies widely at various irradiances and temperatures. The MPP (Maximum Power Point) range of a medium- or high-power PV PCS is normally 450~830Vdc or 300~600Vdc. This means the PV PCS should operate in a wide range of modulation indexes. The PV PCS should satisfy the harmonic current requirement that the TDD (Total demand distortion) shall not exceed 5%. This paper proposes a new PWM control method for a medium- or high-power PV PCS which increases the efficiency of power conversion in all operation ranges with acceptable harmonic ripple currents. This paper compares and analyzes appropriate PWM schemes for the PV PCS in the view points of conversion efficiency and current harmonics.

Keywords: PV PCS, Pulse width modulation, Harmonic loss, Switch loss

1. Introduction

Renewable energy like wind power, solar power and fuel cells is a major and effective solution to the problem of global warming. This is especially true of solar radiation. It is an abundant source of energy, with the amount of solar radiation reaching the earth's surface being 1000 times greater than the energy released by all the fossil fuels currently being consumed. Moreover, photovoltaic systems are a clean and noise-free source of electricity.

Fig. 1 represents a three-phase PWM converter, which is widely used in medium- and high-power renewable energy generation systems such as PV PCSs. Grid-connected renewable energy generation systems should satisfy the harmonic current requirement that the TDD (Total demand distortion) shall not exceed 5% [7]. Also, Grid-connected renewable energy generation systems should have very high efficiency at all load ranges. Since a tradeoff exists between low harmonic currents and high efficiency, Grid-connected PV PCSs should be designed to optimally satisfy the both requirements.

Losses of a power device are classified as conduction losses and switching losses. To minimize the switching

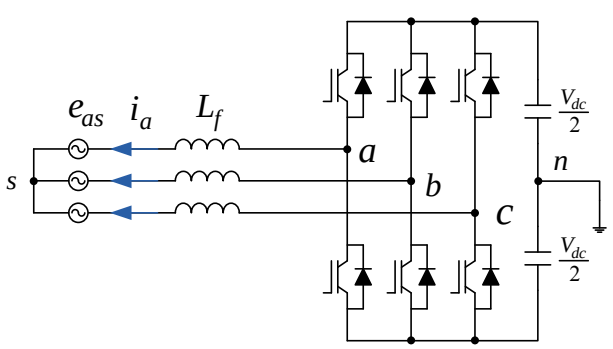

Fig. 1. Three-phase PWM Converter System connected to a grid.

Manuscript received May. 15, 2009; revised Sept. 14, 2009
†Corresponding Author: sjoh68@hanyang.ac.kr
Tel: +82-2-2220-0453, Fax: +82-2-2297-5495, Hanyang Univ.
*Dept. of Automotive Engineering, Hanyang Univ.

losses of three-phase PWM converter systems, lots of PWM schemes have been proposed. A novel PWM strategy based on a space vector PWM has been developed in order to minimize the loss of a voltage-fed three-phase PWM converter in all ranges of the phase angle[1]. This method has shown very good results in the case of its modulation index M which equals almost one.

Meanwhile, the output voltage levels of PV arrays vary widely at various irradiances and temperatures [5-6]. The MPP (Maximum Power Point) range of a medium- or high-power PV PCS is normally from 450Vdc to 830Vdc or from 300Vdc to 600Vdc. Moreover, a PV PCS operates at a range of 88% ~ 110% of the nominal ac grid voltage [7]. This means a PV PCS should operate in a wide range of modulation indexes M . Thus, various PWM schemes are required for PV PCS systems because of the wide operating range of modulation indexes M .

Besides, it is important to select an appropriate L filter in order to decrease the ripple currents of a power conversion system [4]. The ripple current is strongly related to the PWM scheme. Since the resultant ripple current through the L filter and the conversion system causes additional power loss to PV PCS systems, it should be considered in loss calculation.

This paper compares and analyzes appropriate PWM schemes for a PV PCS in terms of conversion efficiency and current harmonics. It also shows why a PV PCS cannot use some discontinuous PWM schemes. Based on the analysis and comparison, this paper proposes a new PWM strategy for medium- and high-power PV PCSs. Experimental results are also included to prove the performance of the proposed method.

2. Circuit Analysis

In Fig. 1, the voltage equation between the a-phase injection current (i_a), the a-phase output voltage of the PWM converter (v_{as}) and the a-phase grid voltage (e_{as}) is as follows:

$$L_f \frac{di_a}{dt} = v_{as} - e_{as} . \tag{1}$$

where $e_{as} = \sqrt{2}E_{as}\sin\omega t$.

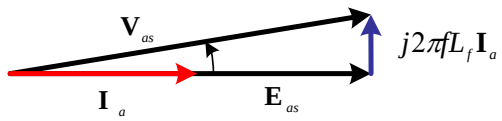

Fig. 2. Relation between grid current and voltages.

If the phase angle of the a-phase grid voltage (e_{as}) is assumed to be zero in steady state, then (1) goes to (2).

$$\begin{aligned} I_a &= \frac{V_{as}\angle\phi_i - E_{as}\angle 0^\circ}{2\pi fL_f} \\ &= \frac{(V_{as}\cos\phi_i - E_{as})\angle 0^\circ + V_{as}\sin\phi_i\angle 90^\circ}{2\pi fL_f} \end{aligned} \tag{2}$$

Fig. 2 shows the relation between the a-phase injection current phasor ($\mathbf{I}_a$), the a-phase output voltage of the PWM converter phasor ($\mathbf{V}_{as}$) and the a-phase grid voltage phasor ($\mathbf{E}_{as}$).

In order to increase the efficiency of energy transfers, renewable energy generation systems like wind power, solar power and fuel cells should be controlled so that the phase angle between the grid voltage and the grid current equal zero. To satisfy this condition, Equalities (3) and (4) are needed as follows:

$$V_{as}\cos\phi_i - E_{as} = 0 \tag{3}$$

$$I_a = \frac{V_{as}\sin\phi_i\angle 90^\circ}{2\pi fL_f} \tag{4}$$

Since $2\pi fL_f << 1[pu]$, we can get $\phi_i \approx 0$ and $V_{as} \approx E_{as}$. Therefore, the output voltage of the PWM converter (V_{as}) and the grid voltage (E_{as}) are almost equal in the steady state, and the output voltage of the PWM converter (V_{as}) is controlled so that its phase (ϕ_i) lags the grid voltage (E_{as}) slightly.

3. PWM Schemes

The pole voltage (v_{an}), the phase voltage (v_{as}) and the offset voltage (v_{sn}) are denoted as shown in Fig. 1, and

their relationships are as follows [1]:

$$v_{an} = v_{as} + v_{sn}, \quad v_{bn} = v_{bs} + v_{sn}, \quad v_{cn} = v_{cs} + v_{sn} \tag{5}$$

In a three-phase PWM scheme, there is one degree of freedom that v_{sn} can be selected as any value on the condition that:

$$-\frac{V_{dc}}{2} < v_{an} < \frac{V_{dc}}{2}, \; -\frac{V_{dc}}{2} < v_{bn} < \frac{V_{dc}}{2}, \; -\frac{V_{dc}}{2} < v_{cn} < \frac{V_{dc}}{2}, \tag{6}$$

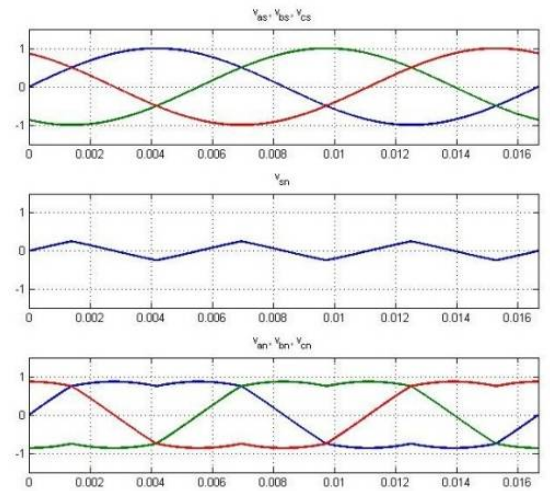

(a)

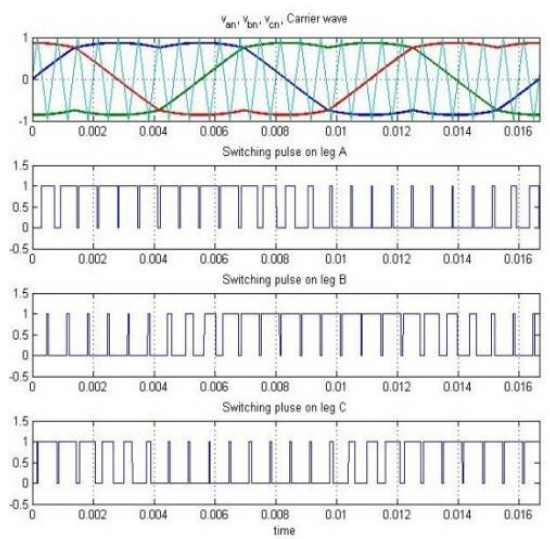

(b)

Fig. 3. Symmetric SVPWM switching pattern; grid frequency=60Hz, switching frequency =1500Hz, modulation index M=1.0, (a) offset voltage of SVPWM, (b) switching pattern of SVPWM.

that is:

$$-\frac{V_{dc}}{2} - v_{\min} < v_{sn} < \frac{V_{dc}}{2} - v_{\max} \tag{7}$$

where $v_{\max} = \max(v_{as}, v_{bs}, v_{cs})$, $v_{\min} = \min(v_{as}, v_{bs}, v_{cs})$. Therefore, numerous PWM schemes can be implemented by selecting v_{sn} appropriately. Fig. 3 demonstrates an example of a symmetric space vector PWM (SVPWM) scheme.

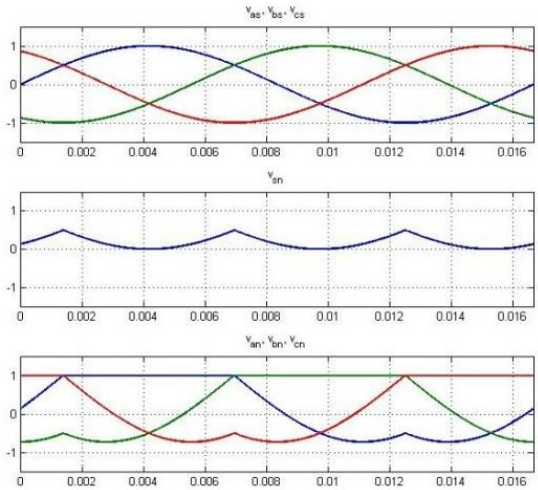

(a)

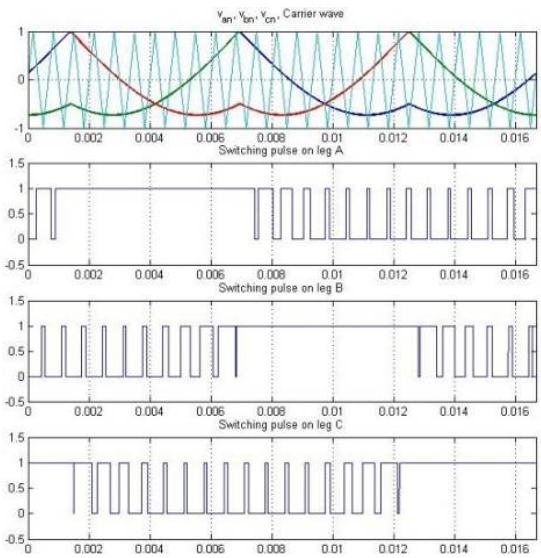

(b)

Fig. 4. 120° discontinuous PWM(DPWMMIN) switching pattern; grid frequency=60Hz, switching frequency =1500Hz, modulation index M=1.0, (a) offset voltage of DPWMMIN, (b) switching pattern of DPWMMIN.

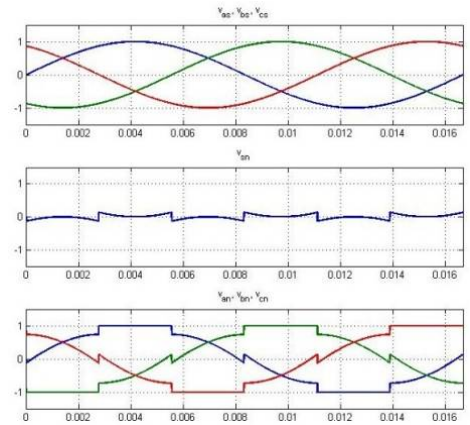

(a)

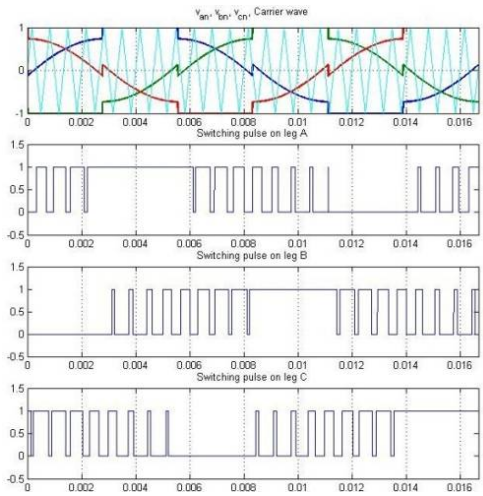

(b)

Fig. 5. 60° discontinuous PWM(DPWM1) switching pattern; grid frequency=60Hz, switching frequency =1500Hz, modulation index M=1.0, (a) offset voltage of DPWM1, (b) switching pattern of DPWM1.

Fig. 4 demonstrates an example of a 120° discontinuous PWM (DPWMMIN) scheme.

Fig. 5 demonstrates an example of a 60° discontinuous PWM(DPWM1) scheme. This method has the smallest switching loss at the phase angle zero ($\phi_i \approx 0$) [1].

4. Current Harmonics

The current harmonics caused by various PWM schemes are analyzed in[2-3]. The analytic calculation of harmonic currents is summarized in this section.

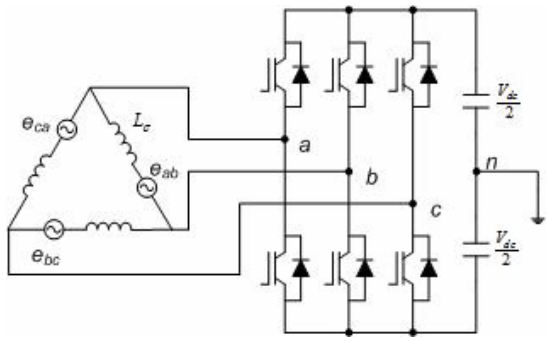

Fig. 6. Equivalent circuit of grid-connected three-phase inverter.

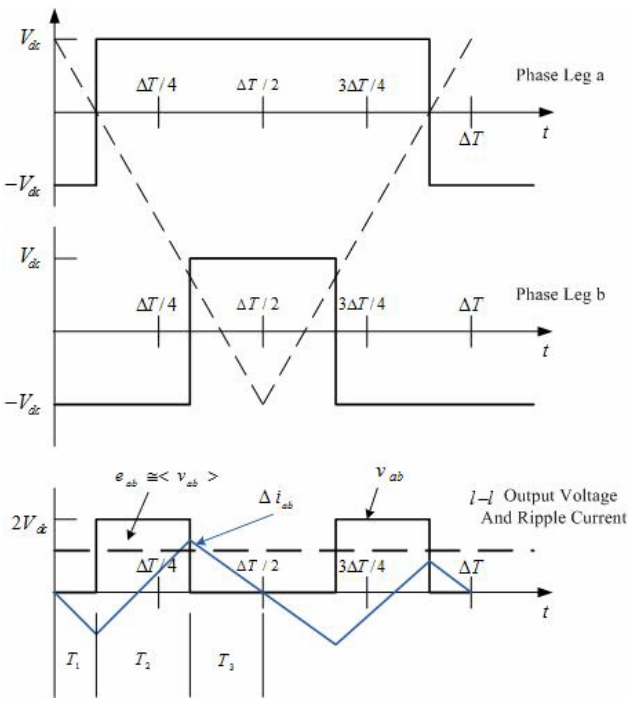

Fig. 7. Modulation process and resulting delta element ripple current for two phase legs of three-phase VSI.

In the case of a three-phase inverter, it is convenient to assume that the inductive load is delta connected to avoid issues associated with zero sequence components (Fig. 6). For a practical case, the currents flowing through the equivalent delta circuit can be readily calculated by means of the usual delta/wye transformation equations.

Fig. 7 shows the sketch of a single carrier switching period with the load between output phase legs a and b. For each of the periods T_1, T_2, T_3, the current ripple (Δi_{ab}) through a delta load element is defined by:

$$0 \le t \le T_1: \quad \Delta i_{ab}(t) = -\frac{e_{ab}}{L_\sigma} t \,, \tag{8}$$

$$T_1 \le t \le T_1 + T_2: \Delta i_{ab}(t) = \left(\frac{2V_{dc} - e_{ab}}{L_\sigma}\right)(t - T_1) - \frac{e_{ab}}{L_\sigma} T_1 \,, \tag{9}$$

$$T_1 + T \le t \le T_1 + T_2 + T_3:$$

$$\Delta i_{ab}(t) = -\frac{e_{ab}}{L_\sigma}(t - T_1 - T_2) + \left(\frac{2V_{dc} - e_{ab}}{L_\sigma}\right)(T_2) - \frac{e_{ab}}{L_\sigma} T_1 \,. \tag{10}$$

After some manipulation, the average squared value of the current ripple over the interval $\Delta T/2$ ($\langle \Delta i_{ab} \rangle$) can be written in the form [3]:

$$\langle \Delta i_{ab}^2 \rangle = \left(\frac{V_{dc}}{L_\sigma}\right)^2 \frac{\Delta T^2}{48} \left\{(u_2 - u_1) + (u_2 - u_1)^3 + (u_2 - u_1)(u_2^3 - u_1^3)\right\}, \tag{11}$$

where $u_1 = \frac{e_a}{V_{dc}}$, $u_2 = \frac{e_b}{V_{dc}}$.

For a three-phase inverter modulated with simple sinusoidal references, the phase leg reference voltages are given by $u_1 = M\cos\theta_0$ and $u_2 = M\cos(\theta_0 - 2\pi/3)$. Substituting these definitions into (11), with θ_0 replaced by θ for brevity, gives:

$$\langle \Delta i_{ab}^2 \rangle = \left(\frac{V_{dc}}{L_\sigma}\right)^2 \frac{\Delta T^2}{48} \left\{ \begin{array}{l} 3M^2 \cos^2(\theta + \frac{\pi}{6}) - 3\sqrt{3} M^3 \cos^3(\theta + \frac{\pi}{6}) \\ -\sqrt{3} M^4 \cos(\theta + \frac{\pi}{6})(\cos^3(\theta - \frac{2\pi}{3}) - \cos^3\theta) \end{array} \right\}. \tag{12}$$

The average RMS harmonic current of a simple sinusoidal PWM can now be determined by integrating (12) over the positive half fundamental cycle of line-line voltage:

$$I_{ab,h,rms}^2 = \left(\frac{V_{dc}}{L_\sigma}\right)^2 \frac{\Delta T^2}{48} \left(\frac{3}{2} M^2 - \frac{4\sqrt{3}}{\pi} M^3 + \frac{9}{8} M^4\right). \tag{13}$$

By calculating the RMS ripple current in the same manner, the RMS ripple currents of various PWM schemes are produced as follows [3]:

SVPWM:

$$I_{ab,h,rms}^2 = \left(\frac{V_{dc}}{L_\sigma}\right)^2 \frac{\Delta T^2}{48} \left(\frac{3}{2} M^2 - \frac{4\sqrt{3}}{\pi} M^3 + \frac{9}{8}(\frac{3}{2} - \frac{9}{8}\frac{\sqrt{3}}{\pi}) M^4\right). \tag{14}$$

DPWMMIN:

$$I_{ab,h,rms}^2 = \left(\frac{V_{dc}}{L_\sigma}\right)^2 \frac{\Delta T^2}{48} \left(6M^2 - \frac{35\sqrt{3}}{2\pi} M^3 + (\frac{27}{8} - \frac{81}{64}\frac{\sqrt{3}}{\pi}) M^4\right). \tag{15}$$

DPWM1:

$$I_{ab,h,rms}^2 = \left(\frac{V_{dc}}{L_\sigma}\right)^2 \frac{\Delta T^2}{48} \left(6M^2 - (\frac{45}{2\pi} + \frac{4\sqrt{3}}{\pi}) M^3 + (\frac{27}{8} + \frac{27}{16}\frac{\sqrt{3}}{\pi}) M^4\right). \tag{16}$$

The harmonic distortion factors ($f(M)$) for the various PWM schemes can be defined as:

$$f(M) = I_{ab,h,rms}^2 \Big/ \left(\frac{V_{dc}}{L_\sigma}\right)^2 \frac{\Delta T^2}{48}. \tag{17}$$

It is clear from Fig. 8 that discontinuous modulation schemes produce greater harmonic distortion and harmonic losses than continuous PWM schemes for the same switching frequency. This is especially true, if the modulation index M is about 0.6. In that case the RMS ripple current increases more than three times.

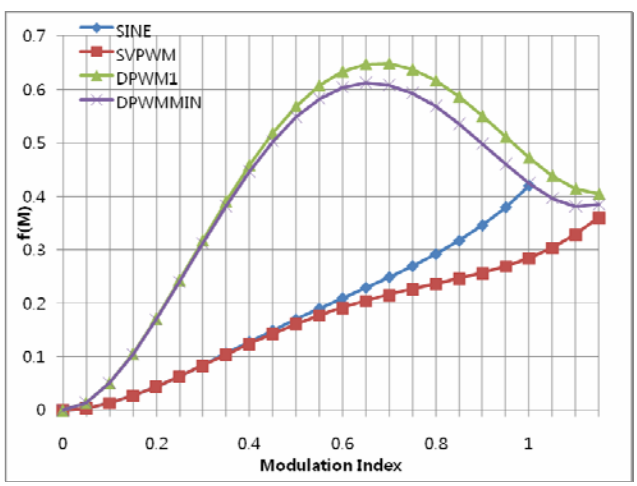

Fig. 8. Harmonic distortion factors against modulation index M for different PWM modulation strategies.

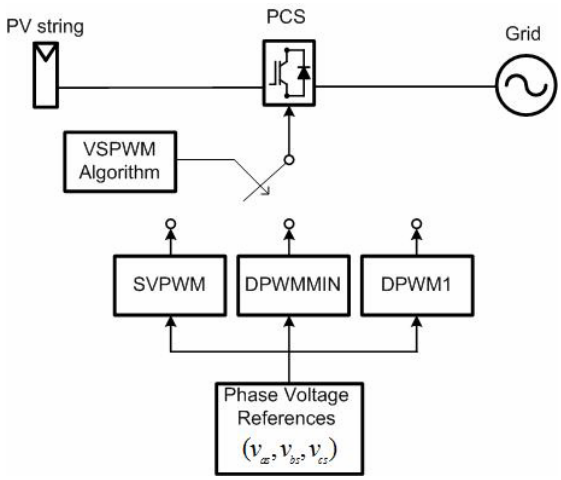

(a)

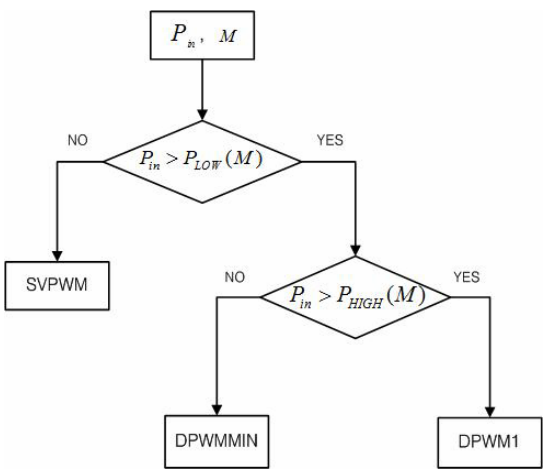

(b)

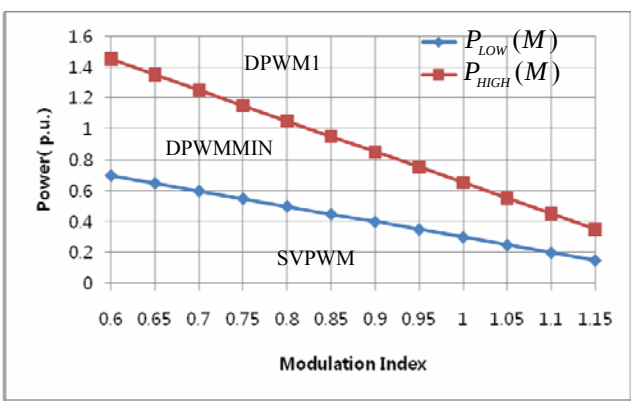

(c)

Fig. 9. Variable Structure PWM (VSPWM) Control scheme, (a) total block diagram of VSPWM, (b) algorithm of VSPWM, (c) power level functions of VSPWM.

5. Variable Structure PWM Control

Since a PV PCS operates in a wide range of modulation indexes M, it is important to determine the best PWM scheme according to the modulation index. Based on previous research [1], it is clear that DPWM1 is the best scheme at high a modulation index (more than 0.9). Unfortunately, this scheme is not appropriate when the modulation index goes down. In that case a PV PCS cannot satisfy the harmonic current requirement that the TDD shall not exceed 5%. However, experiments show that a DPWMMIN scheme can satisfy the harmonic current requirement in the same low modulation index condition. Nevertheless, the SVPWM scheme outperforms the DPWMMIN scheme at a very low modulation index (under 0.6).

If a PV PCS can select appropriate PWM schemes according to the modulation index, the performance of the PV PCS will be increased. Fig. 9 shows the proposed variable structure PWM (VSPWM) scheme. The VSPWM controller selects the SVPWM, DPWMMIN and DPWM1 by comparing the input PV power (P_{in}) with the $P_{LOW}(M)$ and the $P_{HIGH}(M)$ which are power level functions depending on the modulation index M.

6. Experimental Results

6.1 Experimental Setup

Fig. 10 shows the configuration for this experiment. In order to show the performance of the variable structure PWM control strategy, experiments were carried out under the conditions listed in Table 1 and Table 2. To measure the data such as efficiency (η), total harmonic distortion of the grid current (THDi) and power factor (p.f.), a precision power meter LMG500 was used. Fig. 11 shows the implemented PV PCS for this experiment.

6.2 Experimental Results

The VSPWM, SVPWM, and DPWMMIN methods show that each THDi of a 100% load doesn't exceed 5% under the worst conditions (Table 2). However, the DPWM1 method shows that the THDi of a 100% load exceeds 5% under the worst conditions (Table 2).

Table 1. Measurement Data on Vdc=470V.

P_{in}	V_{dc} = 470V			
	DPWM1	DPWMMIN	SVPWM	VSPWM
5kW	η=88.0% THD_i=50.0% p.f.=0.82	η=89.5% THD_i=40.0% p.f.=0.84	η=90.4% THD_i=35.0% p.f.=0.89	η=90.4% THD_i=35.0% p.f.=0.89
10kW	η=94.0% THD_i=25.0% p.f.=0.95	η=94.2% THD_i=22.0% p.f.=0.96	η=94.3% THD_i=20.0% p.f.=0.96	η=94.3% THD_i=20.0% p.f.=0.96
20kW	η=96.3% THD_i=12.0% p.f.=0.98	η=96.5% THD_i=11.0% p.f.=0.99	η=96.3% THD_i=11.0% p.f.=0.99	η=96.5% THD_i=11.0% p.f.=0.99
30kW	η=96.9% THD_i=8.0% p.f.=0.99	η=97.0% THD_i=7.5% p.f.=0.99	η=96.8% THD_i=8.0% p.f.=0.99	η=97.0% THD_i=7.5% p.f.=0.99
40kW	η=97.1% THD_i=5.5% p.f.=1.00	η=97.1% THD_i=6.0% p.f.=1.00	η=97.0% THD_i=5.5% p.f.=1.00	η=97.1% THD_i=5.5% p.f.=1.00
50kW	η=97.1% THD_i=4.5% p.f.=1.00	η=97.1% THD_i=4.5% p.f.=1.00	η=97.1% THD_i=4.5% p.f.=1.00	η=97.1% THD_i=4.5% p.f.=1.00
60kW	η=97.1% THD_i=3.6% p.f.=1.00	η=97.1% THD_i=4.0% p.f.=1.00	η=97.0% THD_i=4.0% p.f.=1.00	η=97.1% THD_i=3.6% p.f.=1.00
70kW	η=97.0% THD_i=3.3% p.f.=1.00	η=97.0% THD_i=3.7% p.f.=1.00	η=96.9% THD_i=3.0% p.f.=1.00	η=97.0% THD_i=3.3% p.f.=1.00
80kW	η=96.9% THD_i=3.0% p.f.=1.00	η=96.9% THD_i=3.3% p.f.=1.00	η=96.7% THD_i=3.0% p.f.=1.00	η=96.9% THD_i=3.0% p.f.=1.00
90kW	η=96.7% THD_i=2.4% p.f.=1.00	η=96.8% THD_i=2.8% p.f.=1.00	η=96.6% THD_i=2.7% p.f.=1.00	η=96.8% THD_i=2.4% p.f.=1.00
100kW	η=96.7% THD_i=2.2% p.f.=1.00	η=96.6% THD_i=2.2% p.f.=1.00	η=96.4% THD_i=2.3% p.f.=1.00	η=96.7% THD_i=2.2% p.f.=1.00

Table 2. Measurement Data on Vdc=830V.

P_{in}	V_{dc} = 830V			
	DPWM1	DPWMMIN	SVPWM	VSPWM
5kW	η=79.0% THD_i=150.0% p.f.=0.52	η=81.5% THD_i=65.0% p.f.=0.77	η=84.7% THD_i=31.3% p.f.=0.92	η=84.7% THD_i=31.3% p.f.=0.92
10kW	η= 88.4% THD_i= 75.0% p.f.=0.79	η=88.2% THD_i=36.0% p.f.=0.91	η=91.9% THD_i=17.0% p.f.=0.98	η=91.9% THD_i=17.0% p.f.=0.98
20kW	η=93.3% THD_i=35.0% p.f.=0.94	η=93.3% THD_i=17.0% p.f.=0.97	η=94.2% THD_i=9.0% p.f.=0.99	η=94.2% THD_i=9.0% p.f.=0.99
30kW	η=94.9% THD_i=24.0% p.f.=0.97	η=94.9% THD_i=13.0% p.f.=0.99	η=95.3% THD_i=7.0% p.f.=1.00	η=95.3% THD_i=7.0% p.f.=1.00
40kW	η=95.5% THD_i=18.0% p.f.=0.98	η=95.5% THD_i=17.0% p.f.=0.99	η=95.8% THD_i=5.0% p.f.=1.00	η=95.8% THD_i=5.0% p.f.=1.00
50kW	η=95.8% THD_i=15.0% p·f=0.99	η=95.8% THD_i=8.0% p·f=1.00	η=96.0% THD_i=4.0% p·f=1.00	η=96.0% THD_i=4.0% p·f=1.00
60kW	η=96.0% THD_i=12.5% p.f.=0.99	η=96.0% THD_i=7.0% p.f.=1.00	η=96.0% THD_i=3.0% p.f.=1.00	η=96.0% THD_i=3.0% p.f.=1.00
70kW	η=96.0% THD_i=10.0% p.f.=0.99	η=96.0% THD_i=5.8% p.f.=1.00	η=96.0% THD_i=3.0% p.f.=1.00	η=96.0% THD_i=3.0% p.f.=1.00
80kW	η=96.0% THD_i=9.4% p.f.=1.00	η=96.0% THD_i=5.0% p.f.=1.00	η=95.9% THD_i=2.5% p.f.=1.00	η=96.0% THD_i=5.0% p.f.=1.00
90kW	η=96.0% THD_i=8.3% p.f.=1.00	η=95.9% THD_i=4.3% p.f.=1.00	η=95.8% THD_i=2.2% p.f.=1.00	η=95.9% THD_i=4.3% p.f.=1.0
100kW	η=95.9% THD_i=7.5% p.f.=1.00	η=95.9% THD_i=4.0% p.f.=1.00	η=95.7% THD_i=1.9% p.f.=1.00	η=95.5% THD_i=4.0% p.f.=1.00

As might be expected, the VSPWM had the best performance for the whole range of operation.

7. Conclusions

A new PWM control strategy which increases the efficiency in all operation ranges with acceptable harmonic ripple currents has been proposed. This method is appropriate for a medium- or high-power PV PCS which is connected to a grid. The appropriate PWM schemes for a PV PCS was compared and analyzed. The reason that a PV PCS cannot use some discontinuous PWM schemes was shown.

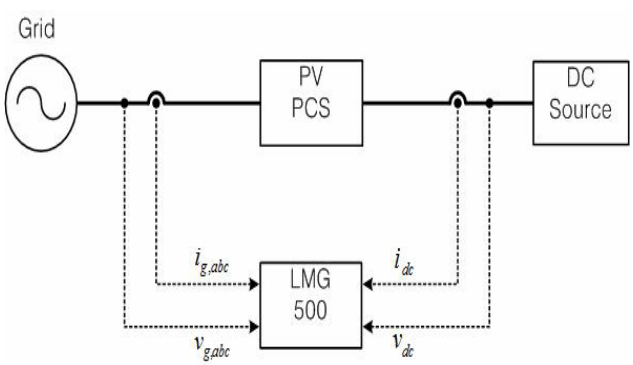

Fig. 10. Measuring data using power meter LMG500.

Fig. 11. Implemented PV PCS.

References

[1] D. W. Jung, S. K. Sul, "Minimum-Loss Strategy for Three-Phase PWM Rectifier," *IEEE Trans. Industrial Electronics,* Vol. 46, pp. 517-526, Jun. 1999.

[2] J. W. Kolar, H. Ertl, and F. C. Zach, "Influence of the modulation method on the conduction and switching losses of a PWM converter system," *IEEE Trans. Industrial Applications,* Vol. 27, pp. 1063-1075, Nov./Dec. 1991.

[3] D. G. Holmes, T. A. Lipo, *Pulse Width Modulation for Power Converters*, NJ: IEEE Press, ch. 4-6, 2003.

[4] Hyosung Kim, "Filter Design for Utility Interactive Inverters using Single-phase Full-bridge Topology," *Journal of KIPE (Korean Institute of Power Electronics)*, Vol. 12, No. 4, pp. 346-353, Aug. 2007.

[5] H. Haeberlin, "Optimum DC Operating Voltage Grid-connected PV Plants," *20th European Photovoltaic Solar Energy Conference,* Barcelona, pp. 1-4, 2005.

[6] B. D. Min, J. P. Lee, J. H. Kim, T. J. Kim, D. W. Yoo, K. R. Ryu, J. J. Kim, E. H. Song, "A Novel Grid-connected PV PCS with New High Efficiency Converter," *The 7th International Conference on Power Electronics*, Daegu, pp. 478-482, 2007.

[7] *IEEE Standard for Interconnecting Distributed Resources with Electric Power Systems*, IEEE Standard 1547, 2003.

Seong-Jin Oh was born in Seoul, Korea in 1968. He received a B.S. degree in mathematics from Kyunghee University, Seoul, Korea, in 1990. He received a M.S. degree in mathematics from POSTECH, Pohang, Korea, in 1992. Since 2005, he has been with Department of Automotive Engineering, Hanyang University, where he is currently a doctoral student. His research interests are in the areas of modeling and control of converters and inverters. Mr. Oh is a member of KIPE (Korean Institute of Power Electronics).

Myoung-Ho Sunwoo was born in Seoul, Korea in 1953. He received a B.S. degree in electrical engineering from Hanyang University, Korea, in 1979. He received a M.S. degree in electrical engineering from University of Texas at Austin, Texas, USA, in 1983. He received a Ph.D. in system engineering from Oakland University, Michgan, USA, in 1990. From 1985 to 1993, he was a researcher with General Motors Research Labs. Since 1993, he has been with the Department of Automotive Engineering, Hanyang University, where he is currently a Professor. Prof. Sunwoo is a member of the Institute of Electrical and Electronics Engineers (IEEE).